AIAA/AAS Astrodynamics Specialist Conference and Exhibit
21 - 24 August 2006, Keystone, Colorado

AIAA 2006-6026

Analytic Solutions for Aerocapture, Descent, and Landing Trajectories for Dual-Use Ballute Systems

Kristin L. Gates Medlock*, Mohammad A. Ayoubi*, James M. Longuski†, and
Purdue University, West Lafayette, Indiana 47907-2023

Daniel T. Lyons‡
Jet Propulsion Laboratory, Pasadena, California 91109-8099

In a dual-use ballute system, we use the ballute first, to aerocapture the orbiter, and second, to soft-land the payload. Using Vinh's analytic theory for aerocapture trajectories, we derive expressions for the maximum heating rates, maximum deceleration, and maximum dynamic pressure as functions of the ballistic coefficient and of the capture trajectory, which in turn provides the required size (area/mass ratio) of the ballute. We follow a similar approach in developing an analytic theory for the ballute-lander. We apply our results to Earth (returns), Mars, Titan, and Neptune.

Nomenclature

C_B	=	ballistic coefficient,
C_D	=	drag coefficient
g	=	gravitational acceleration, m/s^2
m	=	mass, kg
q	=	heating rate, W/cm^2
R	=	radius of the atmosphere, km
R_n	=	nose radius, m
r	=	radial distance, km
S	=	cross-sectional area, m^2
t	=	time, s
v	=	speed, km/s
v_c	=	circular speed, km/s
v_e	=	entry speed, km/s
x	=	non-dimensional speed variable
Z	=	non-dimensional altitude variable
α	=	non-dimensional speed ratio parameter
β	=	inverse scale height, km^{-1}
ϕ	=	non-dimensional flight path angle variable
γ	=	flight path angle, deg
ρ	=	atmospheric density, kg/m^3

I. Introduction

SIGNIFIGANT research has been conducted to investigate the benefits and feasibility of aerocapture and ballute aerocapture at multiple destinations.[1–9] An inflatable ballute system for aerocapture has the potential of providing performance benefits via its large area-to-mass ratio. During ballute aerocapture simulations, it is customary to release the ballute at the appropriate instant and then ignore it to focus on the trajectory of the orbiter. Recent studies[10–12] suggest that, in addition to capturing the orbiter, the ballute may subsequently be used by a

* Doctoral Candidate, School of Aeronautics & Astronautics, 315 North Grant St., Student Member AIAA.
† Professor, School of Aeronautics & Astronautics, 315 North Grant St., Member AAS, Associate Fellow AIAA.
‡ Senior Engineer, Jet Propulsion Laboratory, California Institute of Technology, Mail Stop 301-140L.

descent probe or lander as illustrated in Fig. 1. The dual-use ballute concept has the potential to dramatically alter the way we approach exploration of the Solar System.

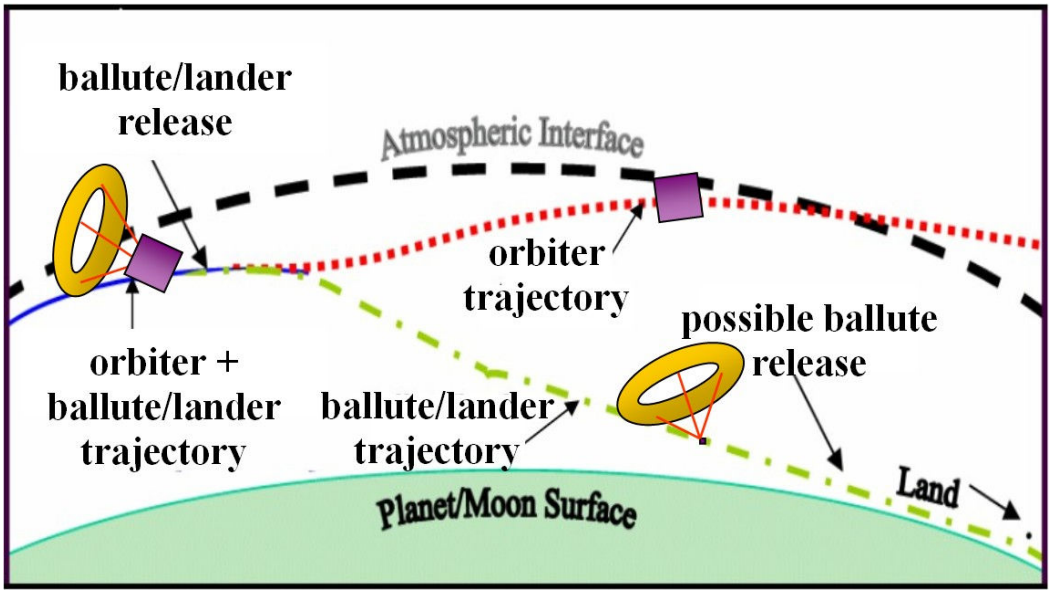

Fig. 1 A schematic of a dual-use ballute trajectory.

It is the purpose of this paper to present an analytical investigation of dual-use ballute trajectories. We provide analytical solutions for both the capture and the landing segments of the dual-use ballute trajectory. In previous work by Vinh et al.,[13] a second-order analytic solution for aerocapture trajectories is derived. Using a similar method, we derive a solution for ballute terminal-descent trajectories. In addition, we use this theory to obtain a ballute sizing algorithm, capable of determining the ballistic coefficient [$=m/(C_D S)$] necessary to maintain heating rates, deceleration, and dynamic pressure below specified limits.

II. Analytic Solutions for Dual-Use Ballute Trajectories

Extensive numerical studies have been carried out for ballistic trajectories with and without drag modulation.[14,15] With only the drag force involved and with the effect of the rotation of the atmosphere neglected, the motion is planar.

$$\frac{dr}{dt} = v\sin\gamma \tag{1}$$

$$\frac{dv}{dt} = \frac{-\rho S C_D v^2}{2m} - g\sin\gamma \tag{2}$$

$$\frac{d\gamma}{dt} = -\frac{1}{v}\left(g - \frac{v^2}{r}\right)\cos\gamma \tag{3}$$

We note that g in Eq. (2) refers to the local gravitational acceleration at a given planet.

The atmosphere is assumed the be locally exponential and is given by

$$d\rho = -\beta(r)\rho dr \tag{4}$$

A. Analytic Solutions for Capture Trajectory

Vinh et al.[13] derive a generalized Yaroshevskii's system of equations for analyzing ballistic entry at super-circular speeds and constant ballistic coefficient. They then provide a second-order analytical solution using Poincaré's method of integration by inserting a small parameter, ε. This approach is appropriate for the entry segment prior to ballute/lander release (and, with rescaling, the remainder of the capture trajectory).

The assumptions given in Eqs. (5)–(6) are applied to Eqs. (1)–(3),

$$\begin{aligned} g(r) &\approx g(R) \\ \frac{v^2}{r} &\approx \frac{v^2}{R} \end{aligned} \tag{5}$$

$$-g\sin\gamma = 0 \tag{6}$$

resulting in the simplified equations of motion presented in Eqs. (7)–(9).

$$\frac{dr}{dt} = v\sin\gamma \tag{7}$$

$$\frac{dv}{dt} = \frac{-\rho S C_d v^2}{2m} \tag{8}$$

$$\frac{d\gamma}{dt} = -\frac{1}{v}\left(g - \frac{v^2}{r}\right)\cos\gamma \tag{9}$$

Vinh uses the non-dimensional variables given in Eqs. (10)–(12), representing altitude, flight path angle, and speed, respectively.

$$Z = \rho S C_D m^{-1}\left(R/\beta\right)^{1/2} \tag{10}$$

$$\phi = -\left(\beta R\right)^{1/2}\sin\gamma \tag{11}$$

$$x = \log\left(v_e^2/v^2\right) \tag{12}$$

An additional non-dimensional variable, α, specifies the type of entry orbit (i.e. hyperbolic: α<0.5, parabolic: α=0.5, elliptic: α>0.5).

$$\alpha = gR/v_e^2 = v_c^2/v_e^2 \tag{13}$$

Dividing the time derivatives of Eqs. (10) and (11) by the time derivative of Eq. (12) and applying the small angle approximation in Eq. (14),

$$\cos\gamma \approx 1 \tag{14}$$

provide equations of motion

$$\frac{dZ}{dx} = \phi \tag{15}$$

$$\frac{d\phi}{dx} = \left(\alpha e^{x} - 1\right) Z^{-1} \tag{16}$$

with initial conditions

$$\begin{aligned} &x = 0, \\ &Z(0) = \varepsilon = \rho_e S C_D m^{-1} \left(R/\beta\right)^{1/2}, \\ &\phi(0) = c = -\left(\beta R\right)^{1/2} \sin\gamma_e \end{aligned} \tag{17}$$

To facilitate integration by use of Poincaré's method of artificially inserting a small parameter, a final change of variables is made,

$$y = Z/\varepsilon \tag{18}$$

$$\tau = x/\varepsilon \tag{19}$$

$$d(\ )/d\tau = (\ )' \tag{20}$$

to obtain Eqs. (21) and (22),

$$y' = \phi \tag{21}$$

$$\phi' = \left(\alpha e^{\varepsilon\tau} - 1\right)/y \tag{22}$$

with initial conditions,

$$\tau = 0, \quad y(0) = 1, \quad \phi(0) = c \tag{23}$$

Using drag parameter ε, we look for solutions of the form:

$$\begin{aligned} y &= y_0 + \varepsilon y_1 + \varepsilon^2 y_2 + \ldots \\ \phi &= \phi_0 + \varepsilon\phi_1 + \varepsilon^2\phi_2 + \ldots \end{aligned} \tag{24}$$

with initial conditions

$$\begin{aligned} &y_0(0) = 1, \quad y_1(0) = y_2(0) = \ldots = 0 \\ &\phi_0(0) = c, \quad \phi_1(0) = \phi_2(0) = \ldots = 0 \end{aligned} \tag{25}$$

Substituting Eq. (24) into Eqs. (15) and (16) and equating like terms of ε, gives the following system of equations:

$$y_0' = \phi_0 \tag{26}$$

$$\phi_0' = -(1-\alpha)\, y_0^{-1} \tag{27}$$

$$y_1' = \phi_1 \tag{28}$$

$$\phi_1' = (1-\alpha)\, y_1 y_0^{-2} + \alpha\tau y_0^{-1} \tag{29}$$

$$y_2' = \phi_2 \tag{30}$$

$$\phi_1' = (1-\alpha)\, y_2 y_0^{-2} - \alpha\tau y_1 y_0^{-2} + \frac{1}{2}\alpha\tau^2 y_0^{-1} - (1-\alpha)\, y_1^2 y_0^{-3} \tag{31}$$

As indicated by Vinh, after some labor, solutions for the 0th, 1st, and 2nd order systems are obtained. (See Refs. 12 and 13 for details). For the convenience of the reader, we provide Vinh's solutions as follows.

1. Zeroth-Order Analytic Solution

The independent variable ϕ_0 (representing the zero-order flight path angle) monotonically increases from its initial value c. The zero-order solution for the altitude variable, y, is

$$y_0 = \exp\left[\left(c^2 - \phi_0^2\right)/\delta\right] \tag{32}$$

where

$$\delta = 2(1-\alpha) \tag{33}$$

represents the entry speed. The analytical expression for τ, representing the speed variable is

$$\tau = \sqrt{\frac{\pi}{\delta}} \exp\left(\frac{c^2}{\delta}\right)\left[erf\left(\frac{c}{\sqrt{\delta}}\right) - erf\left(\frac{\phi_0}{\sqrt{\delta}}\right)\right] \tag{34}$$

where the error function is defined as

$$erf(x) = 2\pi^{-1/2}\int_0^x e^{-t^2}\, dt \tag{35}$$

2. First-Order Analytic Solution

The first-order solution coefficients for y and ϕ are

$$y_1 = 2\alpha\delta^{-2}\phi_0 + 2\alpha\delta^{-2}k\left(y_0 - \phi_0\tau\right) \tag{36}$$

$$\phi_1 = \alpha\delta^{-1}\left(k\tau - 1\right)y_0^{-1} + \alpha\delta^{-1}\left(y_0 - \phi_0\tau\right) \tag{37}$$

where,

$$k = (1-\alpha)\tau - c \tag{38}$$

3. Second-Order Analytic Solution

The second-order solution coefficients for y and ϕ are

$$\begin{aligned} y_2 &= 2\alpha\delta^{-3}\left(y_0-\phi_0\tau\right)\left[\left(1+\alpha\right)+\left(1-\alpha\right)\tau^2\right] \\ &+\alpha\delta^{-3}\phi_0\tau\left[\alpha+\left(\delta/6\right)\left(\alpha+2\right)\tau^2\right] \\ &-\alpha\delta^{-3}\left(\alpha+2\right)y_0^3-\alpha^2\delta^{-3}\left(k\tau-1\right)^2 y_0^{-1} \\ &+\alpha\delta^{-2}ky_1-6\alpha\delta^{-4}\left(\alpha+2\right)\phi_0\left[K\left(\phi_0\right)-K\left(c\right)\right] \end{aligned} \tag{39}$$

$$\begin{aligned} \phi_2 &= 2\alpha\delta^{-2}\left(y_0-\phi_0\tau\right)\tau \\ &+\alpha\delta^{-3}\phi_0\left[\alpha+\left(1+\alpha\right)\left(\alpha+2\right)\tau^2\right] \\ &+\left(\delta/6\right)\delta^{-2}\tau y_0^{-1}\left[3\left(\alpha+2\right)+\left(1-\alpha\right)\left(4-\alpha\right)\tau^2\right] \\ &+\alpha^2\delta^{-3}\left(k\tau-1\right)^2\phi_0 y_0^{-2}+\left(\alpha/2\right)\delta^{-1}y_1+\alpha\delta^{-2}k\phi_1 \\ &-2\alpha^2\delta^{-3}\left(k\tau-1\right)y_0^{-1}\left[k+\left(1-\alpha\right)\tau\right] \\ &+3\alpha\delta^{-3}\left(\alpha+2\right)y_0^{-1}\left[K\left(\phi_0\right)-K\left(c\right)\right] \end{aligned} \tag{40}$$

where,

$$K\left(\phi_0\right)=\left(\delta\pi/12\right)^{1/2}\exp\left(3c^2/\delta\right)erf\left[\left(3/\delta\right)^{1/2}\phi_0\right] \tag{41}$$

4. Numerical Results

In this paper, we consider missions at Earth, Mars, Titan , and Neptune with a wide range of entry conditions. Table 1 provides some specific values for a typical dual-use ballute system in which the ballute area may range from 500-3000 m^2. Numerical results presented throughout this paper use the conditions and parameters displayed in Tables 1 and 2.

Table 1 Vehicle Parameters for Dual-Use Ballute Simulations at Earth, Mars, Titan and Neptune

Parameter	Orbiter	Ballute/Lander
m	400 kg	100 kg
C_D	1.37	1.37
A	2 m^2	500–3000 m^2 *
R_n	0.8 m	15.5 m
C_B	$m/(C_D A)$	0.730–0.122 kg/m^2

* Representative of the ballistic coefficient range used.

The range of entry speeds examined at Earth, Mars, Titan, and Neptune are adapted from previous studies[1,2,8,9,16,17] and are displayed in Table 2.

Table 2 Entry Conditions and Atmospheric Constants at Earth, Mars, Titan, and Neptune

Condition	Earth	Mars	Titan	Neptune
βR	900	350	56	441
reference density, kg/m^2	2.22e-8	4.73e-10	7.52e-10	1.48E-14
Entry/Exit Altitude, km	120	150	1025	1500
Inertial Entry Speeds, km/s	12.9	5.75–11	6.5–10	23.6

We choose an entry flight path angle that targets a circular orbit at exit (assuming the ballute/lander is not released). Because the target apoapsis altitude of the orbiter is higher than that of the chosen circular exit orbit, the ballute/lander will be released inside the atmosphere and continue its descent. This method allows the vehicle to dive deep enough to accommodate navigation and atmospheric uncertainties while maintaining a high enough trajectory to keep the heating rates low.

Figures (2)–(4) depict the accuracy of the analytical solutions compared to the numerical integration of the original planar equations of motion. Vinh's capture theory accurately applies to the segment of the capture trajectory prior to ballute/lander release. At the point of release, changing the ballistic coefficient to that of the orbiter and rescaling the equations accordingly, provides an analytic solution for the remainder of the orbiter's capture trajectory. However, to portray the remaining descent trajectory of the lander, we need a different analytical solution.

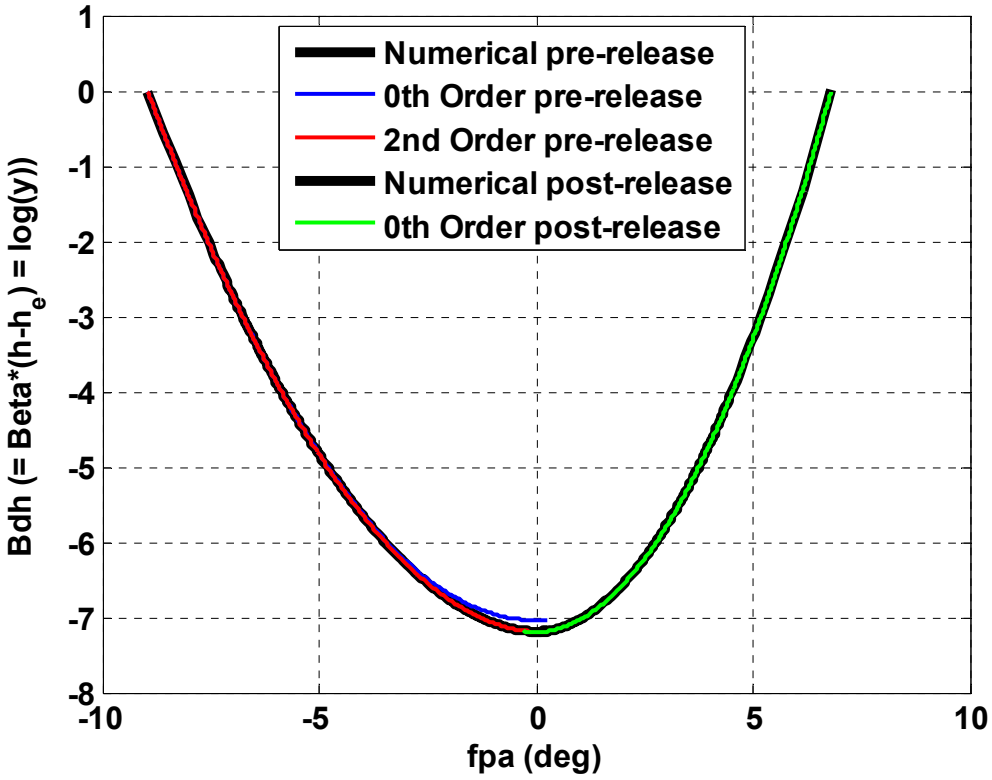

Fig. 2 Variation of linear altitude vs flight path angle.

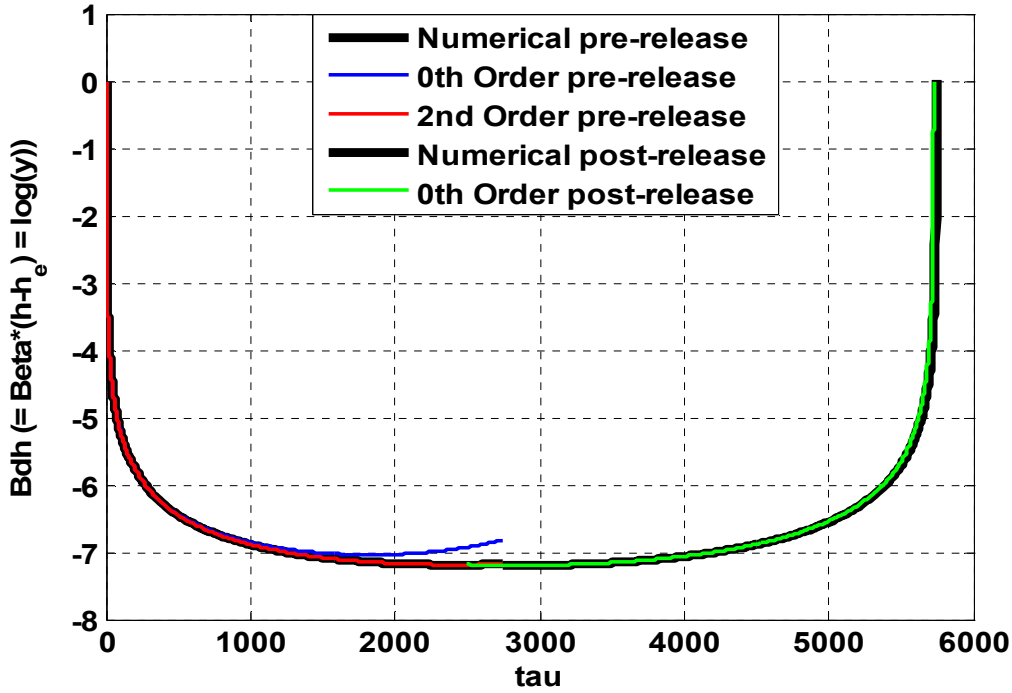

Fig. 3 Variation of linear altitude vs representative speed variable, τ.

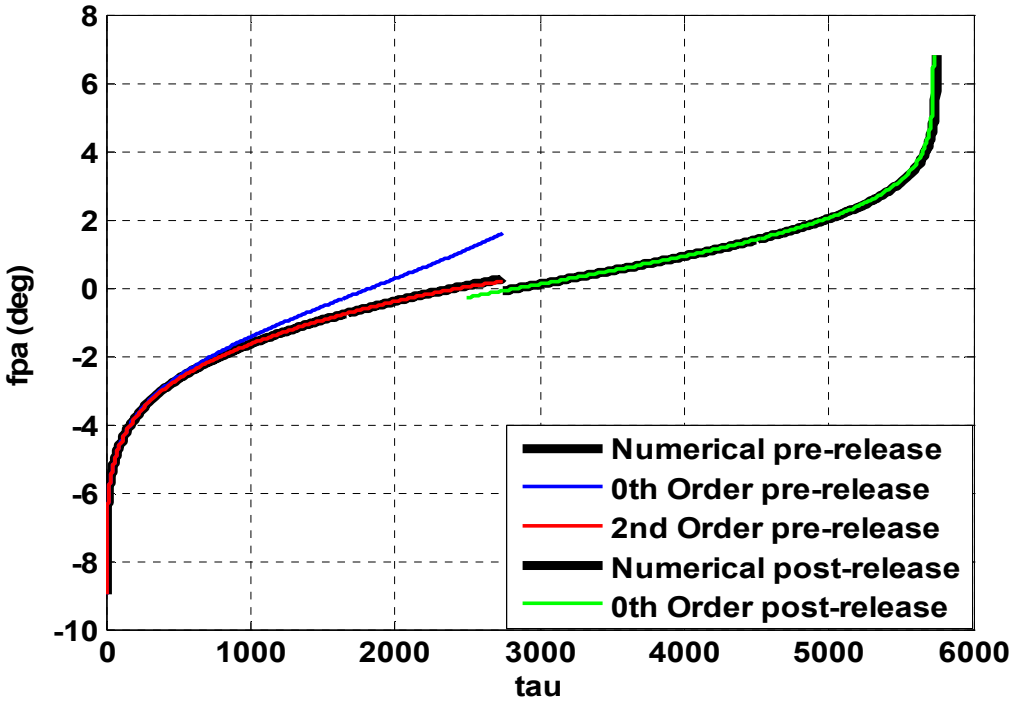

Fig. 4 Flight path angle vs representative speed variable, τ.

B. Analytic Solutions for Descent Trajectory

Vinh's second-order solution discussed in the previous section uses the zero-order flight path angle parameter φ_0 as the independent variable, varying it from c to –c. This theory only applies to skip trajectories (i.e. trajectories that exit the atmosphere).

1. Chapman's Theory

Here we modify Chapman's entry theory[14,18] to apply to ballistic entry (i.e. $C_L=0$). We again start with Eqs. (1)–(3), reiterated here for convenience:

$$\frac{dr}{dt} = v\sin\gamma \tag{42}$$

$$\frac{dv}{dt} = \frac{-\rho S C_D v^2}{2m} - g\sin\gamma \tag{43}$$

$$\frac{d\gamma}{dt} = -\frac{1}{v}\left(g - \frac{v^2}{r}\right)\cos\gamma \tag{44}$$

Dividing Eqs. (43) and (44) by Eq. (42) eliminates t and makes r the independent variable. Setting $C_L=0$ for a ballute trajectory, we have

$$\frac{dv}{dr} = \frac{-\rho S C_D v}{2m\sin\gamma} - \frac{g}{v} \tag{45}$$

$$\frac{d\gamma}{dr} = \left(1 - \frac{gr}{v^2}\right)\frac{\cos\gamma}{r\sin\gamma} \tag{46}$$

Chapman uses two basic assumptions, the second of which applies only to lifting vehicles and is not needed here. His first assumption states that in a given time increment, the fractional change in distance from the planet center is small compared to the fractional change in the horizontal component of velocity. Mathematically, this assumption is expressed as

$$\left|\frac{d\left(v\cos\gamma\right)}{v\cos\gamma}\right| \gg \left|\frac{dr}{r}\right| \tag{47}$$

We use Chapman's variables, where $\overline{u}$ is independent and $\overline{Z}$ is dependent, defined as

$$\overline{u} = \frac{v\cos\gamma}{\sqrt{gr}} \tag{48}$$

$$\overline{Z} = \frac{\rho S C_D}{2m}\sqrt{\frac{r}{\beta}}\,\overline{u} \tag{49}$$

Rewriting the basic assumption in Eq. (47) in terms of the new variables gives

$$\left|\frac{d\left(v\cos\gamma\right)/v\cos\gamma}{dr/r}\right| = \left|1+\frac{\sqrt{\beta r}\bar{Z}}{\bar{u}\sin\gamma}\right| \gg 1 \tag{50}$$

or

$$1 \gg \left|\frac{\bar{u}\sin\gamma}{\sqrt{\beta r}\bar{Z}}\right| \tag{51}$$

Assuming an inverse-square gravity defined by,

$$g = \frac{\mu}{r^2} \tag{52}$$

the derivative of $\bar{u}$ with respect to *r* is

$$\frac{d\bar{u}}{dr} = \frac{\cos\gamma}{\sqrt{gr}}\frac{dv}{dr} - \frac{v\sin\gamma}{\sqrt{gr}}\frac{d\gamma}{dr} + \frac{v\cos\gamma}{2r\sqrt{gr}} \tag{53}$$

Using Eqs. (45), (46), (48), and (49) in Eq. (53) and applying the assumption in Eq. (51), we have

$$\frac{d\bar{u}}{dr} = \frac{\bar{Z}}{\sin\gamma}\sqrt{\frac{\beta}{r}} \tag{54}$$

Taking the derivative of $\bar{Z}$ with respect *r* and applying Eqs. (4) and (54) gives

$$\frac{d\bar{Z}}{dr} = -\frac{\bar{Z}^2}{\bar{u}\sin\gamma}\sqrt{\frac{\beta}{r}} - \beta\bar{Z}\left(1-\frac{1}{2\beta r}+\frac{1}{2\beta^2}\frac{d\beta}{dr}\right) \tag{55}$$

Since βr is large, the last term of Eq. (55) can be approximated by $-\beta\bar{Z}$ and the equation becomes

$$\frac{d\bar{Z}}{dr} = -\frac{\bar{Z}}{\sin\gamma}\sqrt{\frac{\beta}{r}}\left(\frac{\bar{Z}}{\bar{u}}+\sqrt{\beta r}\sin\gamma\right) \tag{56}$$

Now, Eq. (46) is written in terms of Chapman's variables

$$\frac{d\gamma}{dr} = \frac{\bar{Z}}{\bar{u}\sin\gamma}\sqrt{\frac{\beta}{r}}\left[\frac{\bar{u}\cos\gamma}{\sqrt{\beta r}\bar{Z}}\left(1-\frac{\cos^2\gamma}{\bar{u}^2}\right)\right] \tag{57}$$

In order to make $\bar{u}$ the independent variable, Eqs. (56) and (57) are divided by Eq. (53) resulting in the following two equations.

$$\frac{d\bar{Z}}{d\bar{u}} - \frac{\bar{Z}}{\bar{u}} = \sqrt{\beta r}\sin\gamma \tag{58}$$

$$\frac{d\gamma}{d\bar{u}} = -\frac{\cos\gamma}{\sqrt{\beta r}\bar{Z}}\left(1-\frac{\cos^2\gamma}{\bar{u}^2}\right) \tag{59}$$

If we assume βr is constant and take the derivative of Eq. (58) with respect to $\bar{u}$, using Eq. (59), we get

$$\bar{u}\frac{d}{d\bar{u}}\left(\frac{d\bar{Z}}{d\bar{u}}-\frac{\bar{Z}}{\bar{u}}\right)+\frac{\cos^2\gamma\left(\bar{u}^2-\cos^2\gamma\right)}{\bar{Z}\bar{u}}=0 \tag{60}$$

$$\begin{array}{ccccc} \bar{u}\dfrac{d^2\bar{Z}}{d\bar{u}^2} & - & \left(\dfrac{d\bar{Z}}{d\bar{u}}-\dfrac{\bar{Z}}{\bar{u}}\right) & = & \dfrac{\left(1-\bar{u}^2\right)}{\bar{Z}\bar{u}}\cos^4\gamma \\ \text{Vertical} & & \text{Vertical component} & & \text{Gravity minus} \\ \text{acceleration} & & \text{of drag force} & & \text{centrifugal force} \end{array} \tag{61}$$

$$\bar{u}\frac{d}{d\bar{u}}\left(\frac{d\bar{Z}}{d\bar{u}}-\frac{\bar{Z}}{\bar{u}}\right)=\frac{\left(1-\bar{u}^2\right)}{\bar{Z}\bar{u}}\cos^4\gamma \tag{62}$$

Equation (61) displays Chapman's form of the solution with vertical acceleration, vertical component of drag force, and gravity minus centrifugal force components labeled appropriately.[8] Equation (62) is another form of the solution. Equations (61) and (62) are obtained by rearranging Eq. (60) and reapplying his basic assumption.

Equations (58) and (61) are the modified Chapman equations, where Eq. (58) is used to evaluate the flight path angle.

2. Yaroshevskii's Solution

Here we modify Yaroshevskii's entry solution[14,19,20] to apply to our problem of ballistic entry ($C_L=0$). For constant lift and drag coefficients, Yaroshevskii's variables are

$$\bar{x} = \ln\left(\frac{\sqrt{gr_o}}{v}\right) \tag{63}$$

$$\bar{y} = \frac{1}{2}C_B^{-1}\sqrt{\frac{r_o}{\beta}}\rho \tag{64}$$

where the subscript *o* indicates conditions at a reference level..

Using a constant reference value for *r* and assuming a very small flight path angle, Chapman's variables, Eqs. (48) and (49), can be written as

$$\bar{u} = \frac{v}{\sqrt{g_o r_o}} \tag{65}$$

$$\bar{Z} = \frac{\rho S C_D}{2m}\sqrt{\frac{r_o}{\beta}}\,\bar{u} \tag{66}$$

The relationships between Yaroshevskii's and Chapman's variables are

$$\frac{\bar{Z}}{\bar{u}} = \bar{y} \tag{67}$$

$$\bar{u} = e^{-\bar{x}} \tag{68}$$

and the relationships between the derivatives are

$$\frac{d}{d\bar{u}}(\ ) = -e^{\bar{x}}\frac{d}{d\bar{x}}(\ ) = \frac{1}{\bar{u}}\frac{d}{d\bar{x}}(\ ) \tag{69}$$

Applying Eqs. (67)–(69) to Chapman's Eq. (61), gives the identical form of Yaroshevskii's equation simplified for ballistic entry,

$$\frac{d^2\bar{y}}{d\bar{x}^2} = \frac{e^{2\bar{x}} - 1}{\bar{y}} \tag{70}$$

Yaroshevskii assumes entry at circular speed with $\rho_e=0$, resulting in the following initial conditions:

$$\bar{x}_i = 0, \quad \bar{y}(0) = 0, \quad \bar{y}'(0) = 0 \tag{71}$$

For small values of x, Eq. (70) can be approximated as,

$$\bar{y}\bar{y}'' = 2\bar{x} \tag{72}$$

which, satisfying Eq. (71), has the following solution.

$$\bar{y} = \sqrt{\frac{8}{3}}\bar{x}^{3/2} \tag{73}$$

Therefore, solutions of Eq. (70) have the form

$$\bar{y} = \sqrt{\frac{8}{3}}\bar{x}^{3/2}\left(a_0 + a_1\bar{x} + a_2\bar{x}^2 + a_3\bar{x}^3 + \ldots\right) \tag{74}$$

Rewriting Eq. (70) using Eq. (74)

$$\bar{y}\bar{y}'' = 2\bar{x} + 2\bar{x}^2 + \frac{4}{3}\bar{x}^3 + \frac{2}{3}\bar{x}^4 + \ldots \tag{75}$$

and equating like powers of $\bar{x}$, we find

$$a_0 = 1, \quad a_1 = \frac{1}{6}, \quad a_2 = \frac{1}{24}, \quad a_3 = \frac{47}{4752}, \ \ldots \tag{76}$$

where the coefficients a_k are calculates using,

$$a_k = \frac{\dfrac{2^k}{(k+1)!} - \dfrac{1}{3}\sum_{m=1}^{k-1}(2m+1)(2m+3)a_m a_{k-m}}{1+(2k+1)(2k+3)/3} \tag{77}$$

Yaroshevskii's solution assumes that the initial speed is circular. If after release the ballute/lander is traveling at super-circular speed, $\bar{x}$ is negative as defined by Eq. (63) and Eq. (74) is invalid until circular speed is reached. Yaroshevskii also assumes that the initial altitude is at atmospheric entry ($\rho=0$, $\bar{y}=0$). We discover that a good heuristic solution is created by simply adding the initial $\bar{y}$ condition at circular speed to the solution in Eq. (74).

$$\bar{y} = \bar{y}_c + \sqrt{\frac{8}{3}}\bar{x}^{3/2}\left(a_0 + a_1\bar{x} + a_2\bar{x}^2 + a_3\bar{x}^3 + \ldots\right) \tag{78}$$

3. Solution for Landing Trajectories Starting at Super-Circular Speeds

To evaluate the segment of the trajectory immediately following release, we return to Vinh's Eqs. (15) and (16), rewritten as

$$\frac{dZ}{dx} = \phi \tag{79}$$

$$\frac{d\phi}{dx} = \frac{d}{dx}\left(\frac{dZ}{dx}\right) = \left(\alpha e^x - 1\right)Z^{-1} \tag{80}$$

We integrate Eq. (80), assuming that $Z=Z_i$ (constant),

$$\phi - \phi_i = Z_i^{-1}\int_{x_i}^{x}\left(\alpha e^x - 1\right)dx \tag{81}$$

$$\phi = \phi_i + Z_i^{-1}\left[\alpha e^x - \alpha e^x - x + x_i\right] \tag{82}$$

We now substitute Eq. (82) into Eq. (79) and integrate the resulting equation

$$\int_{Z_i}^{Z} dZ = \int_{x_i}^{x}\left[\phi_i + Z_i^{-1}\left(\alpha e^x - \alpha e^{x_i} - x + x_i\right)\right]dx \tag{83}$$

$$Z - Z_i = \phi_i\left(x - x_i\right) + Z_i^{-1}\left[\left(\alpha e^x - \alpha x e^{x_i} - \frac{x^2}{2} + x_i x\right) - \left(\alpha e^{x_i} - \alpha x_i e^{x_i} - \frac{x_i^2}{2} + x_i^2\right)\right] \tag{84}$$

When $x_i=0$, Eq. (84) becomes

$$Z - Z_i = \phi_i x + Z_i^{-1}\left[\alpha\left(e^x - x - 1\right) - \frac{x^2}{2}\right] \tag{85}$$

Another way to integrate Eq. (79) is to assume ϕ_i is small and $Z_i=Z$ (i.e. Z is changing). Equation (83) can now be written as

$$\int_{Z_i}^{Z} Z dZ = \int_{x_i}^{x} \left(\alpha e^{x} - \alpha e^{x_i} - x + x_i \right) dx \tag{86}$$

$$\frac{Z^2 - Z_i^2}{2} = \left(\alpha e^{x} - \alpha x e^{x_i} - \frac{x^2}{2} + x_i x \right) - \left(\alpha e^{x_i} - \alpha x_i e^{x_i} - \frac{x_i^2}{2} + x_i^2 \right) \tag{87}$$

$$Z^2 = Z_i^2 + \left(2\alpha e^{x} - 2\alpha x e^{x_i} - x^2 + 2x_i x \right) - \left(2\alpha e^{x_i} - 2\alpha x_i e^{x_i} - x_i^2 + 2x_i^2 \right) \tag{88}$$

When $x_i=0$, Eq. (88) becomes

$$Z^2 = Z_i^2 + \left[2\alpha \left(e^{x} - x - 1 \right) - x^2 \right] \tag{89}$$

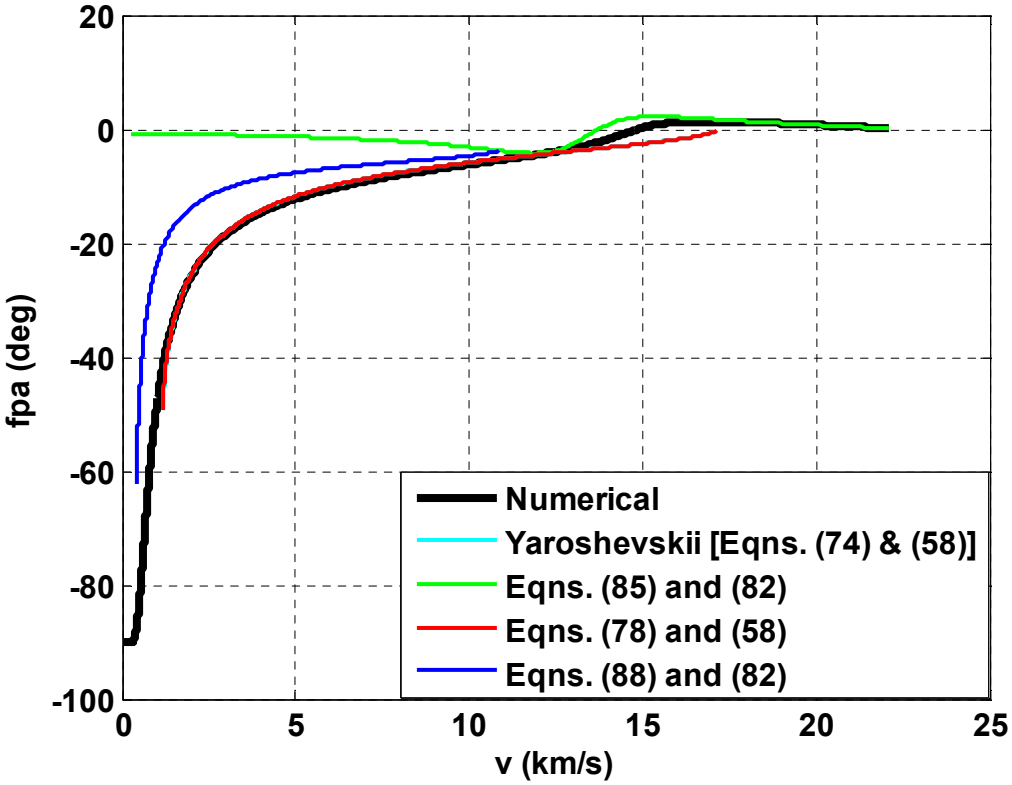

Fig. 5 Flight path angle vs velocity. A comparison of numerical and analytical solutions for descent at Neptune.

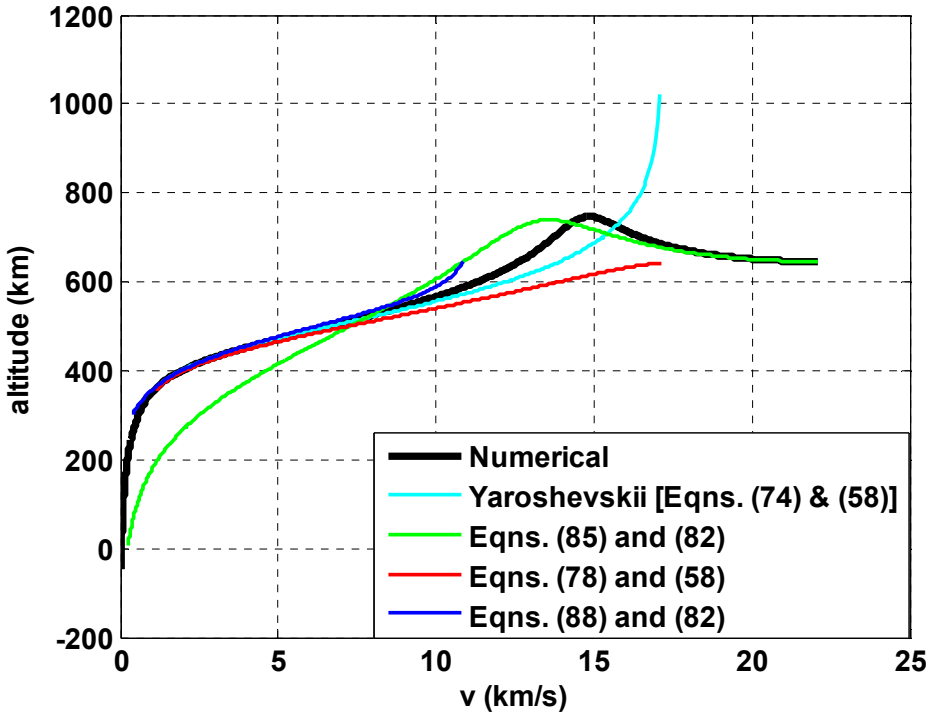

Fig. 6 Altitude vs velocity. A comparison of numerical and analytical solutions for descent at Neptune.

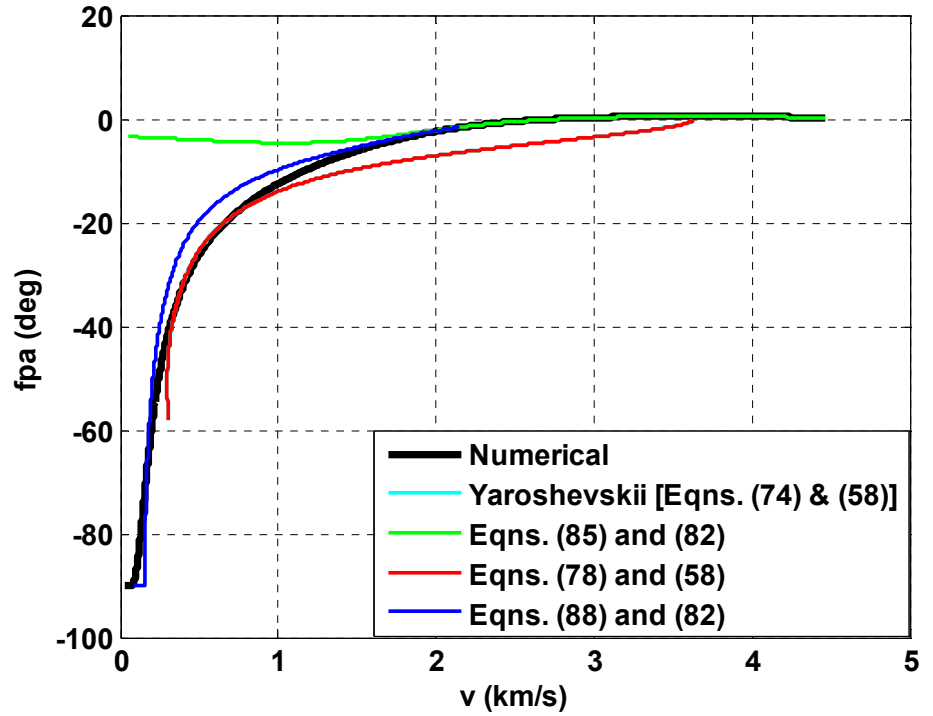

Fig. 7 Flight path angle vs velocity. A comparison of numerical and analytical solutions for descent at Mars.

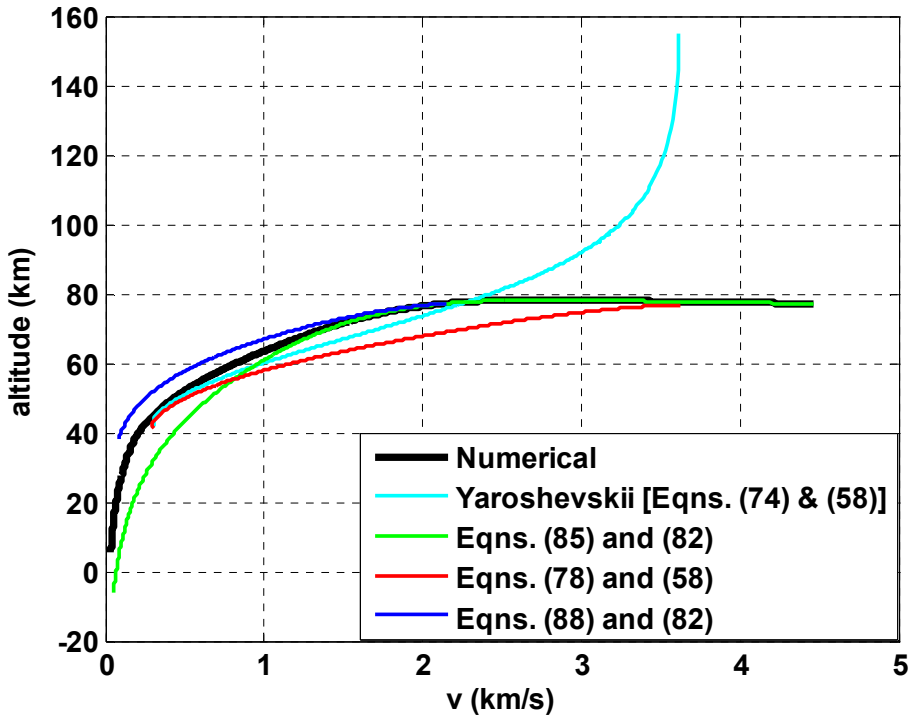

Fig. 8 Altitude vs velocity. A comparison of numerical and analytical solutions for descent at Mars.

Figures (5) and (6) display a comparison between the numerically integrated solution and several analytical solutions for a Neptune dual-use ballute descent trajectory. Figures (7) and (8) show the same comparison for a mission at Mars. Equations (85) and (82) show adequate agreement [green contour in Figs. (5)-(8)] for altitude and flight path angle as functions of speed, until circular speed is reached.

For altitude analysis below circular speed, Eq. (85) follows the numerical trend of an altitude increase (a noticeable blip in the Neptune case) prior to final descent [see Figure (6)] and can be used until the altitude returns to the initial release altitude. (After this point, the altitude changes significantly and the assumption of small change in altitude used to derive Eq. (85) becomes invalid.) Subsequently, as the altitude monotonically decreases from the release altitude we use Eq. (88) (in dark blue). (The reason that Eq. (88) cannot be used before this point is that the small values of $\bar{Z}$, due to the altitude blip, cause Eq. (88) to have imaginary roots.)

For flight path angle analysis below circular speed, Yaroshevskii's flight path angle solution shows good agreement for both the Neptune case and the Mars case [red contour in Figs. (5) and (7), respectively] . Also, for the case at Mars, Eq. (82) used with Eq. (88) displays good accuracy [dark blue contour in Fig. (7)].

III. Peak Conditions During Dual-Use Ballute Trajectories

During a dual-use ballute trajectory, the ballute/lander is typically released just after periapsis, but we note that peak heating rates occur prior to periapsis. In prior work,[17] we show that the lander is typically subjected to the highest g-load, immediately after release, but these loads are not technologically challenging. Using the analytical solutions for ballistic capture trajectories, we obtain expressions for maximum heating rates, maximum deceleration (prior to release), and maximum dynamic pressure, as a functions of the ballistic coefficient and the capture trajectory. Subsequently, these expressions can be used to alter the ballistic coefficient in order to achieve given (i.e. acceptable) heating rates, deceleration, and pressure.

A. Stagnation-Point Heating Rate

Stagnation-point heating rate during atmospheric flight is calculated by,

$$Q_{stag} = \frac{C\rho^{Nstag} v^{Mstag}}{\sqrt{R_n}} \tag{90}$$

(similar to the Sutton-Graves convective heating equation[21]). In Eq. (90), N_{stag} and M_{stag} are the density and velocity coefficients (typical values of N_{stag} = 0.5 and M_{stag} = 3.0 are used for this study), and C is the stagnation point heating coefficient. The stagnation-point heating coefficient (C) varies according to the planet. We use 9.748 x 10^{-5}, 9.80 x 10^{-5}, 9.00 x $10^{-5}$and 3.54 x 10^{-5} $kg^{0.5}$/m for Earth, Mars, Titan and Neptune, respectively. The R_n of the ballute/lander is calculated assuming a spherical ballute.

Eq. (90) can be rewritten as

$$Q_{stag} = C\left(\frac{\rho_e}{R_n}\right)^{1/2} v_e^3 \left(\frac{\rho}{\rho_e}\right)^{1/2} \left(\frac{v}{v_e}\right)^3 \tag{91}$$

From Eqs. (10), (12), (18), and (19), we see that,

$$\frac{\rho}{\rho_e} = y \tag{92}$$

and

$$\frac{v}{v_e} = e^{-\tau\varepsilon/2} \tag{93}$$

Substituting Eqs. (92) and (93) into Eq. (91) gives an expression for stagnation point heating rate as a function of the nondimensional variables y, τ, and ε (representing altitude, speed, and ballistic coefficient, respectively):

$$Q_{stag} = C\left(\frac{\rho_e}{R_n}\right)^{1/2} v_e^3 y^{1/2} e^{-3\tau\varepsilon/2} \tag{94}$$

To evaluate conditions at the point of maximum instantaneous heating rate, we differentiate Eq. (94) with respect to the speed variable τ.

$$\frac{d\left(Q_{stag}\right)}{d\tau} = y' y^{-1/2} e^{-3\tau\varepsilon/2} - 3\varepsilon y^{1/2} e^{-3\tau\varepsilon/2} = 0 \tag{95}$$

Recalling that $y' = \phi$, Eq. (95) simplifies to

$$\phi = 3\varepsilon y \tag{96}$$

Eq. (96) provides the key that relates the speed variable, flight path angle variable, and ballistic coefficient at the point of peak heating. Substituting this equation into the nondimensional heating rate expression, in Eq. (94), gives an equation for maximum heating rate as a function of ϕ:

$$Q_{stag,\max} = C\left(\frac{\rho_e}{R_n}\right)^{1/2} v_e^3 \left(\frac{\phi}{3\varepsilon}\right)^{1/2} e^{-3\tau\varepsilon/2} \tag{97}$$

In order to solve for ϕ in Eq. (97), we derive an expression for ϕ_0, at the point of peak heating. Using Eq. (96) and the zero-order solution for y given in Eq. (32), we obtain an implicit (or transcendental) expression for ϕ_0:

$$\phi_0 = 3\varepsilon y_0 = 3\varepsilon \exp\left[\left(c^2 - \phi_0^2\right)/\delta\right] \tag{98}$$

We see that ϕ_0 appears on both sides of the equation and that an explicit expression for ϕ_0 is not possible. Using the approximation,

$$\exp\left(-\phi_0^2/\delta\right) \approx 1 - \frac{\phi_0^2}{\delta} \tag{99}$$

we obtain an (approximate) explicit expression for ϕ_0, that can be used as an initial guess for solving the implicit expression in Eq.(98).

$$\phi_0 \approx \frac{-\delta}{6\varepsilon}\left[\exp\left(-c^2/\delta\right) - \sqrt{\exp\left(-2c^2/\delta\right) - \frac{36\varepsilon^2}{\delta}}\right] \tag{100}$$

We can now use Eq. (98) with Eqs. (32)–(41) and Eq. (24) to obtain 0th, 1st, and 2nd order solutions for y and ϕ at the point of peak stagnation-point heating in terms of the ballistic coefficient (represented by ε) and the entry conditions (α, representing entry speed, and c, representing entry flight path angle). Depending on the desired accuracy, any order of the ϕ solution can be used in Eq. (96) to determine the appropriate ballute size (ε value) for a given maximum stagnation-point heating rate limit.

Figure 9 shows the ballistic coefficient (calculated using the area of the ballute) plotted against the maximum stagnation point heating rate of the ballute (calculated using an R_n that varies with the ballute size). Similarly, Fig. 4 provides values for the orbiter ($R_n = 0.8$ m^2). Assuming a maximum heating limit of 5 W/cm^2 on the ballute, Fig. 3 indicates that any of the ballute sizes shown will work (the most cost effective, of course, being the smallest). However, applying the same heating limit to the orbiter, Fig.4 shows that only the lowest of the entry velocity cases at Mars and Titan stay within the limit (for the sizes plotted), suggesting that a thermal protection system (TPS) may be required on the orbiter. It is interesting to note that the cases for Titan with $v_e = 6.50$ km/s and Mars with $v_e = 5.75$ km/s follow nearly the same contour. Numerical and analytical results for missions to Neptune and return missions to the Earth (e.g. from the Moon) indicate heating error trends similar to those at Mars and Titan.

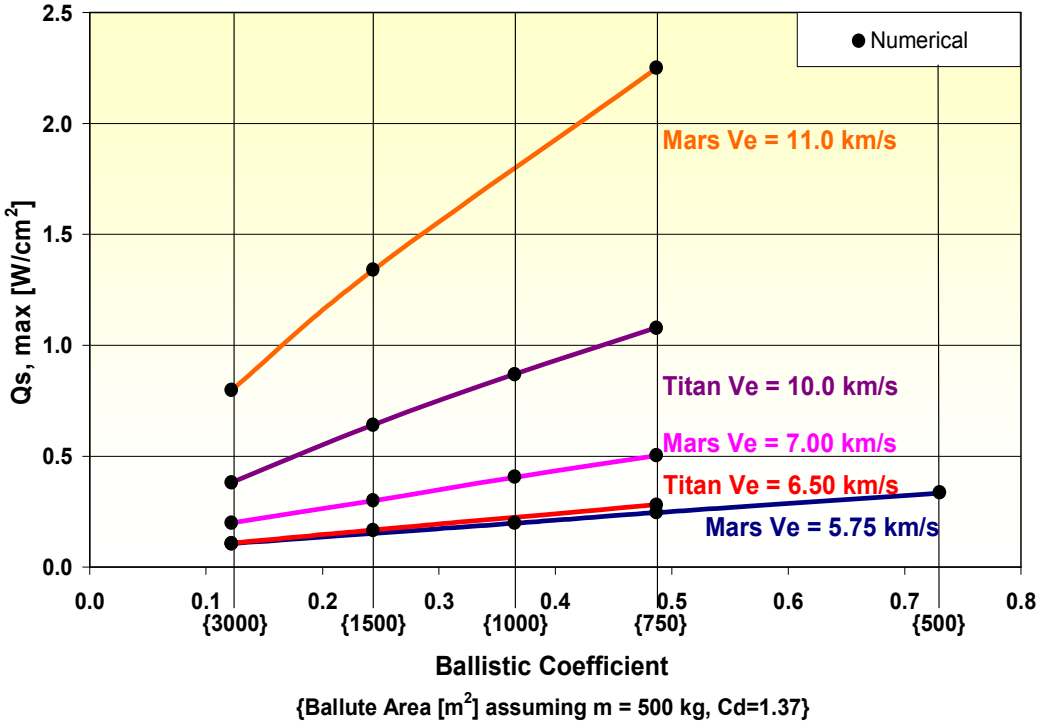

Fig. 9 Maximum stagnation point heating rate (on ballute) vs ballistic coefficient.

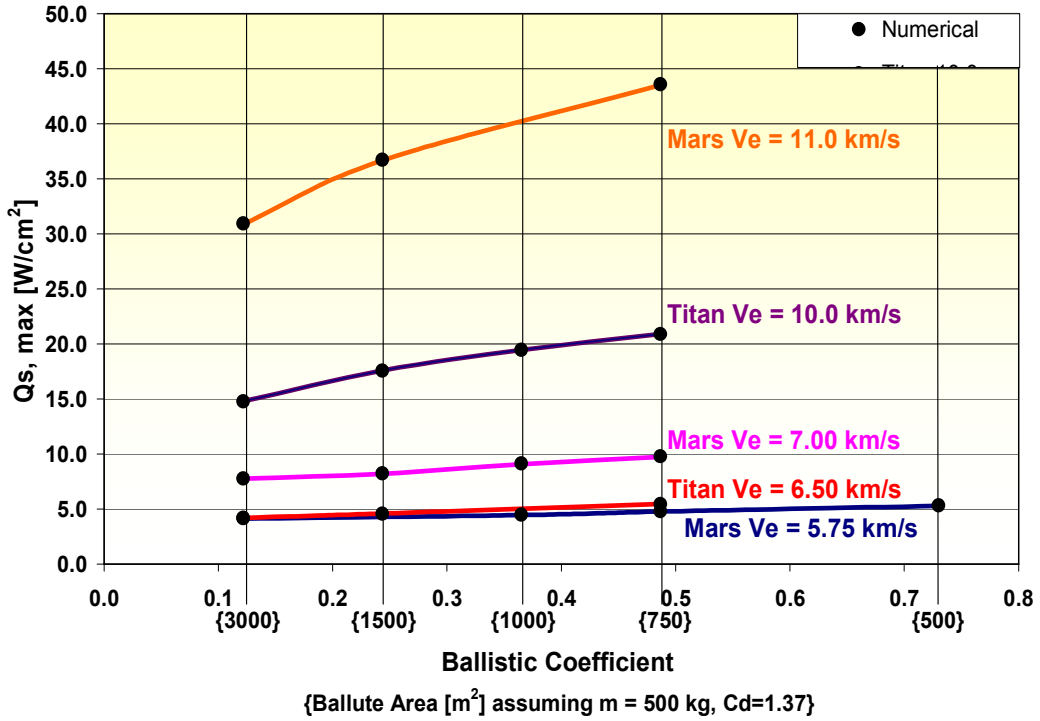

Fig. 10 Maximum stagnation point heating rate (on orbiter) vs ballistic coefficient.

C. Free-Molecular Heating Rate

Free-molecular heating rate is defined as

$$Q_{fm} = \frac{1}{2}\rho v^3 \tag{101}$$

which can also be written as

$$Q_{fm} = \frac{1}{2}\rho_e v_e^3 \left(\frac{\rho}{\rho_e}\right)\left(\frac{v}{v_e}\right)^3 \tag{102}$$

Applying Eqs.(92) and (93) to Eq.(102) gives us an expression for the free-molecular heating rate as follows

$$Q_{fm} = \frac{1}{2}\rho_e v_e^3 y e^{-3\tau\varepsilon/2} \tag{103}$$

To evaluate conditions at the point of maximum free-molecular heating rate, we differentiate Eq.(103).

$$\frac{d\left(Q_{fm}\right)}{d\tau} = y' e^{-3\tau\varepsilon/2} - \frac{3}{2}\varepsilon y e^{-3\tau\varepsilon/2} = 0 \tag{104}$$

Reducing Eq.(104) gives us the following relation at the point of peak free-molecular heating rate

$$\phi = \frac{3}{2}\varepsilon y \tag{105}$$

Eq. (105) provides the key that relates the speed variable, flight path angle variable, and ballistic coefficient at the point of peak free-molecular heating. Substituting this equation into the nondimensional heating rate expression, in Eq. (103), gives an equation for maximum heating rate as a function of ϕ:

$$Q_{fm,\,\max} = \frac{1}{2}\rho_e v_e^3 \left(\frac{2\phi}{3\varepsilon}\right) e^{-3\tau\varepsilon/2} \tag{106}$$

In order to solve for ϕ in Eq. (106), we derive an expression for ϕ_0, at the point of peak heating. Using Eq. (105) and the zero-order solution for y given in Eq. (32), we obtain an implicit (or transcendental) expression for ϕ_0:

$$\phi_0 = \frac{3}{2}\varepsilon y_0 = \frac{3}{2}\varepsilon \exp\left[\left(c^2 - \phi_0^2\right)/\delta\right] \tag{107}$$

Applying the approximation in Eq.(99) to Eq.(107) we obtain an (approximate) explicit expression for ϕ_0, that can be used as an initial guess for solving the implicit expression in Eq. (107).

$$\phi_0 \approx \frac{-\delta}{3\varepsilon}\left[\exp\left(-c^2/\delta\right) - \sqrt{\exp\left(-2c^2/\delta\right) - \frac{9\varepsilon^2}{\delta}}\right] \tag{108}$$

We now use Eq. (107) with Eqs.(32)–(41) and Eq. (24) to obtain 0th, 1st, and 2nd order solutions for y and ϕ at the point of peak free-molecular heating in terms of the ballistic coefficient (represented by ε) and the entry conditions (α, representing entry speed, and c, representing entry flight path angle). Depending on the desired accuracy, any order of the ϕ solution can be used in Eq. (105) to determine the appropriate ballute size (ε value) for a given maximum free-molecular heating rate limit. Figure (11) displays the maximum free-molecular heating rate as a function of ballistic coefficient (similar to the Figures shown for stagnation-point heating rates).

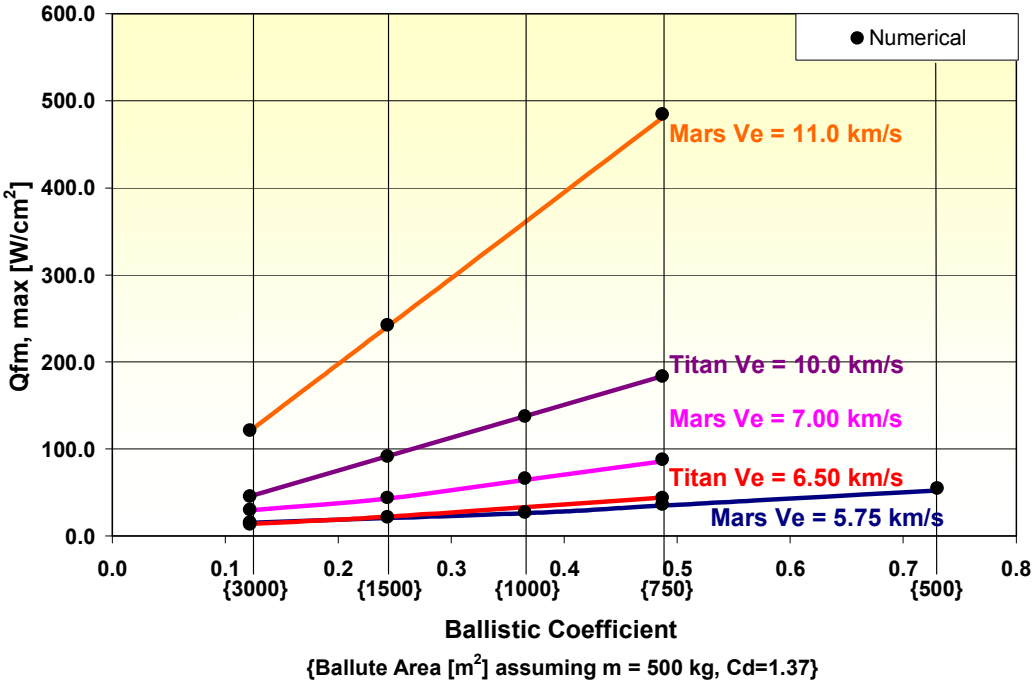

Fig. 11 Maximum free-molecular heating rate vs ballistic coefficient.

D. Deceleration and Dynamic Pressure

Equations (86) and (87) are the definitions of linear deceleration and dynamic pressure, respectively.

$$a/g = \frac{1}{2g} C_B^{-1} \rho v^2 \tag{109}$$

$$P = \frac{1}{2} \rho v^2 \tag{110}$$

These equations can be rewritten as follows:

$$a/g = \frac{\varepsilon}{2\alpha} (\beta R)^{1/2} \left(\frac{\rho}{\rho_e} \right) \left(\frac{v}{v_e} \right)^2 \tag{111}$$

$$P = \frac{1}{2} \left(\frac{\rho_e}{v_e^2} \right) \left(\frac{\rho}{\rho_e} \right) \left(\frac{v}{v_e} \right)^2 \tag{112}$$

Applying Eqs. (92) and (93) to Eqs. (111) and (112) gives us expressions for deceleration and dynamic pressure in terms of Vinh's variables.

$$a/g = \frac{\varepsilon}{2\alpha}\left(\beta R\right)^{1/2} y e^{-\tau\varepsilon} \tag{113}$$

$$P = \frac{1}{2}\left(\frac{\rho_e}{v_e^2}\right) y e^{-\tau\varepsilon} \tag{114}$$

To evaluate conditions at the point of maximum deceleration, we differentiate Eq. (113). Likewise, conditions at the point of maximum dynamic pressure are observed by differentiating Eq. (114). As expected (from the similar ρv^2 terms in found in Eqs. (109) and (110)) differentiating Eqs. (113) and (114) result in the same equality.

$$\frac{d\left(a/g\right)}{d\tau} = \frac{dP}{d\tau} = y' e^{-\tau\varepsilon} - \varepsilon y e^{-\tau\varepsilon} = 0 \tag{115}$$

Reducing Eq. (115) gives us the following identical relation at the points of peak deceleration and peak dynamic pressure, indicating that the two events occur simultaneously.

$$\phi = \varepsilon y \tag{116}$$

Eq. (116) provides the key that relates the speed variable, flight path angle variable, and ballistic coefficient at the point of peak free-molecular heating. Substituting this equation into the nondimensional deceleration and pressure expressions, in Eqs. (113) and (114), gives equations for maximum deceleration and maximum dynamic pressure as functions of ϕ:

$$\left(a/g\right)_{\max} = \frac{\varepsilon}{2\alpha}\left(\beta R\right)^{1/2}\left(\frac{\phi}{\varepsilon}\right) e^{-\tau\varepsilon} \tag{117}$$

$$P_{\max} = \frac{1}{2}\left(\frac{\rho_e}{v_e^2}\right)\left(\frac{\phi}{\varepsilon}\right) e^{-\tau\varepsilon} \tag{118}$$

In order to solve for ϕ in Eqs. (117) and (118), we derive an expression for ϕ_0, at the point of peak deceleration and pressure. Using Eq. (116) and the zero-order solution for y given in Eq. (32), we obtain an implicit (or transcendental) expression for ϕ_0:

$$\phi_0 = \varepsilon y_0 = \varepsilon e^{c^2/\delta} e^{-\phi_0^2/\delta} \tag{119}$$

Applying the approximation in Eq. (99) to Eq. (119) we obtain an explicit expression for ϕ_0, that can be used as an initial guess for solving the implicit expressions in Eqs. (117) and (118).

$$\phi_0 \approx \frac{-\delta}{2\varepsilon}\left[\exp\left(-c^2/\delta\right) - \sqrt{\exp\left(-2c^2/\delta\right) - \frac{4\varepsilon^2}{\delta}}\right] \tag{120}$$

We now use Eq. (117) or Eq. (118), with Eqs. (32)–(41) and Eq. (24) to obtain 0^{th}, 1^{st}, and 2^{nd} order solutions for y and ϕ at the point of peak deceleration or peak dynamic pressure, respectively. Depending on the desired accuracy, any order of the ϕ solution can be used in Eq. (116) to determine the appropriate ballute size (ε value) for a given maximum deceleration limit or maximum pressure limit, prior to release.

Figure (12) displays the maximum deceleration prior to release as a function of ballistic coefficient. It is interesting to note that, for ballute areas between 750 m^2 and 1500 m^2, the maximum deceleration is nearly constant for given entry speeds at Mars and Titan. In the case of Mars with v_e= 7.00 km/s, there is a significant increase in deceleration for decreasing ballistic coefficient (as ballute area increases from 1500 m^2 to 3000 m^2). Whereas the ballute can significantly reduce maximum heating rate, it does not reduce maximum deceleration.

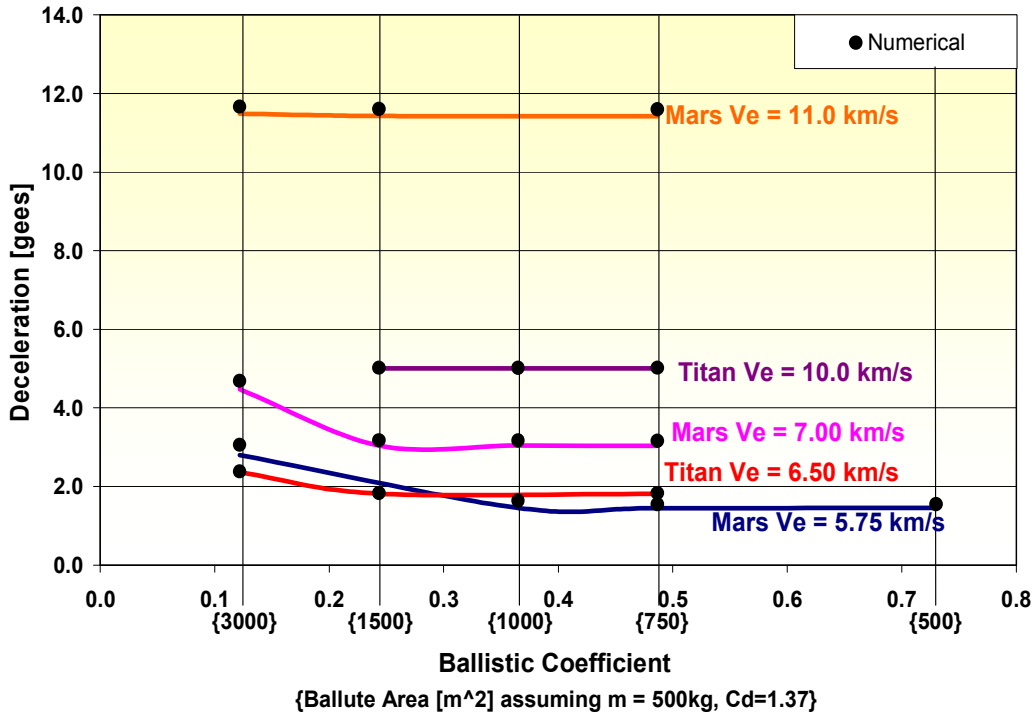

Fig. 12 Maximum deceleration vs ballistic coefficient.

Figure (13) shows the maximum dynamic pressure as a function of the ballistic coefficient for various entry speeds at Mars and Titan. Similar to the stagnation-point heating rate and free-molecular heating rate analyses, maximum dynamic pressure can be greatly reduced by increasing ballute size.

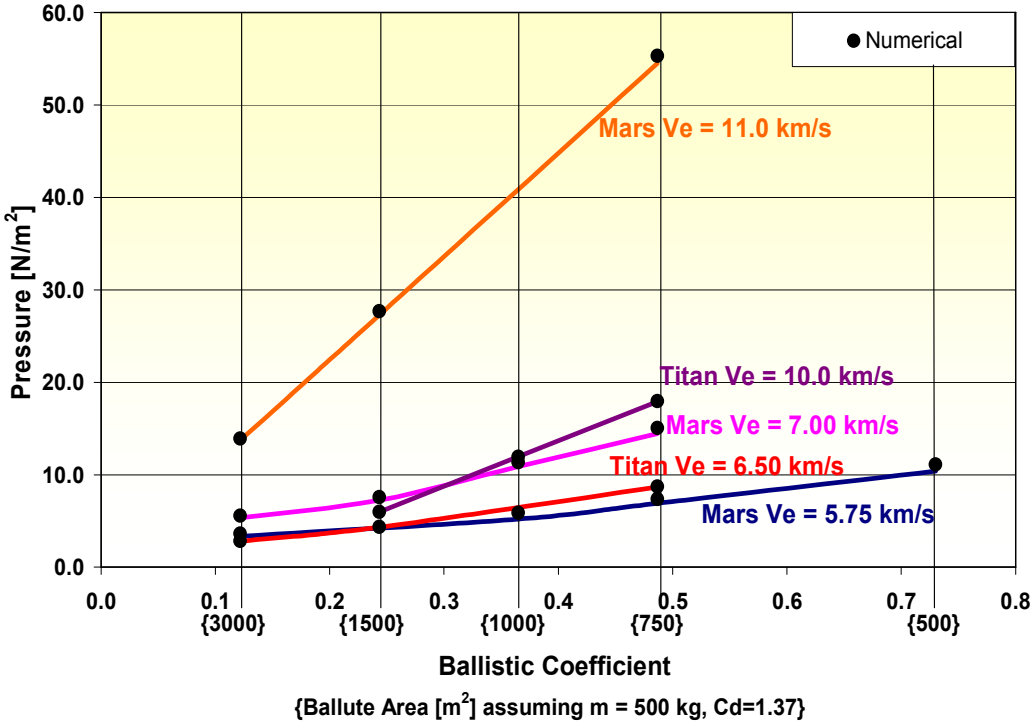

Fig. 13 Maximum dynamic pressure vs. ballistic coefficient.

IV. Conclusions

Based on prior analytical work by Vinh and on new analytical solutions provided in this paper, we are able to find explicit expressions for peak conditions of heating, deceleration, and dynamic pressure for the dual-use ballute. Separate analytical theories are required to account for the aerocapture trajectory of the orbiter and for the descent of the probe (or lander). Our analysis indicates that the peak heating condition for the aerocapture of the orbiter + lander require much greater capabilities (in terms of heat shielding) than for the probe (or lander). Thus, if aerocapture can be achieved with the orbiter + probe then the heating requirements for the probe descent are easily achieved. These capabilities are driven mainly by (and are proportional to) the ballistic coefficient. (In prior work,[12] we show that the lander is typically subjected to the highest g-load, immediately after release, but these loads are not technologically challenging). Preliminary numerical results indicate that (if the area-to-mass ratio can be made large enough) the dual-use ballute promises feasible missions at Mars, Titan, for Earth return, and at Neptune.

Acknowledgments

This work is sponsored in part by a NASA Graduate Student Research Program (GSRP) fellowship from Marshall Space Flight Center (MSFC), under contract number NNM05ZA11H, and by the Jet Propulsion Laboratory (JPL), California Institute of Technology. We would like to thank the In-Space Propulsion Team for their support, especially Bonnie F. James (GSRP Technical Advisor), Erin H. Richardson, and Michelle M. Munk of MSFC. Also, we are grateful to Angus D. McRonald (of Global Aerospace Corporation) for his valuable assistance and advice.

References

[1] Lyons, D. T., and Johnson, W. R., "Ballute Aerocapture Trajectories at Titan," AAS/AIAA Astrodynamics Conference, Big Sky, Montana, American Astronautical Society, AAS Paper 03-646, Aug. 2003.

[2] Lyons, D. T., and Johnson, W. R., "Ballute Aerocapture Trajectories at Neptune," AIAA Atmospheric Flight Mechanics Conference and Exhibit, Providence, RI, AIAA Paper 2004-5181, Aug. 16-19, 2004.

[3] Johnson, W. R., and Lyons, D. T., "Titan Ballute Aerocapture Using a Perturbed TitanGRAM Model," AIAA Atmospheric Flight Mechanics Conference and Exhibit, Providence, RI, AIAA Paper 2004-5280, Aug 16-19, 2004.

[4] Miller, K. L., Gulick, D., Lewis, J., Trochman, B., Stein, J., Lyons, D. T., and Wilmoth, R., "Trailing Ballute Aerocapture: Concept and Feasibility Assessment," 39th AIAA/ASME/ASEE Joint Propulsion Conference and Exhibit, Huntsville, AL, AIAA Paper 2003-4655, July 20-23, 2003.

[5] McRonald, A. D., "A Light-Weight Inflatable Hypersonic Drag Device for Planetary Entry," Association Aeronautique de France Conf. at Arcachon France, March 16-18, 1999.

[6] McRonald, A. D., "A Light-Weight Inflatable Hypersonic Drag Device for Venus Entry," AAS/AIAA Astrodynamics Specialist Conference, Girdwood, Alaska, American Astronautical Society, AAS Paper 99-355, Aug. 16-19, 1999.

[7] McRonald, A. D., "A Light-Weight Inflatable Hypersonic Drag Device for Neptune Orbiter," AAS/AIAA Space Flight Mechanics Meeting, Clearwater, FL, American Astronautical Society, AAS Paper 00-170, Jan. 23-26, 2000.

[8] Lyons, D. T., and McRonald, A. D., "Entry, Descent and Landing using Ballutes," 2nd International Planetary Probe Workshop, NASA Ames Research Center, Moffet Field, CA, Aug. 2004.

[9] Vaughan, D., Miller, H. C., Griffin, B., James, B. F., Munk, M. M., "A Comparative Study of Aerocapture Missions with a Mars Destination," 41st AIAA/ASME/SAE/ASEE Joint Propulsion Conference & Exhibit, Tucson, AZ, AIAA Paper 2005-4110, July 10-13, 2005, pp. 1-16.

[10] Richardson, E. H., Munk, M. M., James, B. F., Moon, S. A., "Review of NASA In-Space Propulsion Technology Program Inflatable Decelerator Investments," 18th AIAA Aerodynamic Decelerator Systems Technology Conference and Seminar, Munich, Germany, AIAA Paper 2005-1603, May 23-26, 2005, pp.1-6.

[11] Gates, K. L., Longuski, J. M., and Lyons, D. T., "A Dual-Use Ballute for Entry and Descent During Planetary Missions," 3rd International Planetary Probe Workshop, Attica, Greece, June 27 – July 1, 2005.

[12] Medlock, K. L. Gates and Longuski, J. M., "An Approach to Sizing a Dual-Use Ballute System for Aerocapture, Descent and Landing," 4th International Planetary Probe Workshop, Pasadena, CA, June 27-30, 2006.

[13] Vinh, N. X., Johannesen, J. R., Longuski, J. M., and Hanson, J. M., "Second-Order Analytic Solutions for Aerocapture and Ballistic Fly-Through Trajectories," *The Journal of the Astronautical Sciences*, Vol. 32, No. 4, Oct.-Dec. 1984.

[14] Vinh, N. X., Busemann, A., and Culp, R. D., *Hypersonic and Planetary Entry Flight Mechanics*, The University of Michigan Press, Ann Arbor, MI, 1980.

[15] Kechichian, J. A., Cruz, M. I., Vihn, N. X., and Rinderle, E. A., "Optimization and Closed-Loop Guidance of Drag-Modulated Aeroassisted Orbital Transfer," AIAA Paper 82-1378, AIAA 9th Atmospheric Flight Mechanics Conference, San Diego, CA, August 1982.

[16] Hall, J. L. and Le, A. K., "Aerocapture Trajectories for Spacecraft with Large, Towed Ballutes," 11th Annual AAS/AIAA Space Flight Mechanics Meeting, Santa Barbara, CA, AAS 01-235, Feb. 11-15, 2001.

[17] Westhelle, C. H. and Masciarelli, J. P., "Assessment of Aerocapture Flight at Titan Using a Drag-only Device," 2003 AIAA Atmospheric Flight Mechanics Conference and Exhibit, Austin, TX, AIAA Paper 2003-5389, Aug. 11-14, 2003.

[18] Chapman, D. R., "An Approximate Analytical Method for Studying Entry into Planetary Atmospheres," NASA TR R-11, 1959.

[19] Yaroshevskii V. A., "The Approximate Calculation of Trajectories of Entry into the Atmosphere I.", Translated from *Kosmicheskie Issledovaniya*, Vol. 2, No. 4, 1964.

[20] Yaroshevskii V. A., "The Approximate Calculation of Trajectories of Entry into the Atmosphere II.", Translated from *Kosmicheskie Issledovaniya*, Vol. 2, No. 5, 1964.

[21] Sutton, K. and Graves, R. A., Jr., "A General Stagnation Point Convective Heating Equation for Arbitrary Gas Mixtures," NASA TR R-376, NASA Langley Research Center, Hampton, VA, Nov. 1971.